THE JOURNAL OF BIOLOGICAL CHEMISTRY VOL. 280, NO. 44, pp. 37098–37106, November 4, 2005

Inactivation of Organellar Glutamyl- and Seryl-tRNA Synthetases Leads to Developmental Arrest of Chloroplasts and Mitochondria in Higher Plants*[S]

Received for publication, May 2, 2005, and in revised form, August 1, 2005 Published, JBC Papers in Press, August 16, 2005, DOI 10.1074/jbc.M504805200

Yu-Kyung Kim[‡1], Jae-Yong Lee[§1], Hye Sun Cho[‡], Sang Sook Lee[‡2], Hyun Jung Ha[¶], Sunghoon Kim[‖], Doil Choi[‡3], and Hyun-Sook Pai[§4]

From the [‡]Laboratory of Plant Genomics, Korea Research Institute of Bioscience and Biotechnology, Taejon 305-333, Korea, the [§]Division of Bioscience and Bioinformatics, Myongji University, Yongin, Kyonggi-do 449-728, Korea, the [¶]Department of Biochemistry, Chungbuk University, Cheongju, Chungcheongbuk-do, Korea, and the [‖]National Creative Research Initiatives Center for ARS Network, Seoul National University, Seoul 151-742, Korea

Aminoacyl-tRNA synthetases (ARSs) are key enzymes involved in protein translation, and both cytosolic and organellar forms are present in the genomes of eukaryotes. In this study, we investigated cellular effects of depletion of organellar forms of ARS using virus-induced gene silencing (VIGS) in *Nicotiana benthamiana*. VIGS of *NbERS* and *NbSRS*, which encode organellar GluRS and SerRS, respectively, resulted in a severe leaf-yellowing phenotype. The *NbERS* and *NbSRS* genes were ubiquitously expressed in plant tissues, and induced in response to light. Green fluorescent protein (GFP) fusion proteins of the full-length glutamyl-tRNA synthetase (ERS) and seryl-tRNA synthetase (SRS) of *Arabidopsis* and GFP fusions to the N-terminal extension of these proteins were all dual-targeted to chloroplasts and mitochondria. At the cell level, depletion of NbERS and NbSRS resulted in dramatically reduced numbers of chloroplasts with reduced sizes and chlorophyll content. The numbers and/or physiology of mitochondria were also severely affected. The abnormal chloroplasts lacked most of the thylakoid membranes and appeared to be degenerating, whereas some of them showed doublet morphology, indicating defective chloroplast division. Pulse-field gel electrophoresis analyses demonstrated that chloroplast DNA in subgenomic sizes is the predominant form in the abnormal chloroplasts. Interestingly, despite severe abnormalities in chloroplasts and mitochondria, expression of many nuclear genes encoding chloroplast- or mitochondria-targeted proteins, and chlorophyll biosynthesis genes remained unchanged in the ERS and SRS VIGS lines. This is the first report to analyze the effect of ARS disruption on organelle development in plants.

Aminoacyl-tRNA synthetases (ARSs)[5] play a critical role in protein synthesis by catalyzing the addition of amino acids to their cognate tRNAs (1, 2). The specificity of aminoacyl-tRNA synthesis in pairing the appropriate tRNAs and amino acids is a key determinant in faithful transmission of genetic information. Despite the crucial function of ARSs in protein synthesis, there are only limited reports on function and regulation of the ARS genes and proteins in plants (3). Protein synthesis in plants takes place in the cytosol, mitochondria, and chloroplasts, and these compartments do not require full sets of unique ARSs encoded by separate nuclear genes. In general, plant ARSs are classified into two groups based on their substrate specificity: the cytosolic enzymes that most efficiently aminoacylate plant or yeast cytosolic tRNAs, and the organellar enzymes that aminoacylate organelle or *Escherichia coli* tRNAs (4).

Recent research has uncovered an extensive degree of sharing of ARS isoforms between compartments, between cytosol and mitochondria or between plastids and mitochondria (5). For example, the cytosolic and mitochondrial leucyl-tRNA synthetases of *Phaseolus vulgaris* aminoacylate cytosolic and mitochondrial $tRNAs^{Leu}$ with equal efficiency but do not aminoacylate chloroplast and *E. coli* $tRNAs^{Leu}$ (6). In addition, AlaRS, ValRS, and ThrRS of *Arabidopsis* are dual targeted to both the cytosol and mitochondria, and the same gene encodes both the mitochondrial and the cytosolic enzyme in each case (7, 8). Dual targeting to mitochondria and chloroplasts has also been observed for HisRS (9), MetRS (10, 11), AsnRS (10), CysRS (10), and one of the GlyRS enzymes (12) in *Arabidopsis*.

Phenotypes of several mutants with defects in ARS gene structure or expression have been characterized in *Arabidopsis*. A tDNA insertion mutant of the cytosolic and mitochondrial AlaRS showed an embryonic lethal phenotype (13). Embryo development of this mutant was arrested at the globular stage with altered patterns of cell division and differentiation. Altered expression of a cytosolic ValRS in plant tissues also caused severe defects in early embryogenesis in the *twn2* mutant in *Arabidopsis* (14). In this mutant, development of apical cells is arrested at a very early stage, and the basal cells proliferate abnormally, giving rise to multiple embryos. Taken together, these results show that cytosolic ARS activity is indispensable in plant cell viability and development. To

* This work was supported by grants from the Plant Diversity Research Center of the 21st Century Frontier Research Program (to H.-S. P. and D. C.) and the Molecular and Cellular BioDiscovery Program (H.-S. P.), which are funded by the Ministry of Science and Technology of the Korean government. The costs of publication of this article were defrayed in part by the payment of page charges. This article must therefore be hereby marked "*advertisement*" in accordance with 18 U.S.C. Section 1734 solely to indicate this fact.

The nucleotide sequence(s) reported in this paper has been submitted to the GenBank™/EBI Data Bank with accession number(s) AAY18610.

[S] The on-line version of this article (available at http://www.jbc.org) contains supplemental Figs. S1 and S2.

[1] Both authors contributed equally to this work.

[2] Present address: Dept. of Genetics, 445 Henry Mall, University of Wisconsin-Madison, Madison, WI 53706-1574.

[3] To whom correspondence may be addressed: Tel.: 82-42-860-4340; Fax: 82-42-860-4309; E-mail: doil@kribb.re.kr.

[4] To whom correspondence may be addressed: Tel.: 82-31-330-6191; Fax: 82-31-335-8249; E-mail: hspai@mju.ac.kr.

[5] The abbreviations used are: ARSs, aminoacyl-tRNA synthetases; ERS, glutamyl-tRNA synthetase; SRS, seryl-tRNA synthetase; IRS, isoleucyl-tRNA synthetase; c-IRS, cytoplasmic isoleucyl-tRNA synthetase; Rubisco, ribulose-bisphosphate carboxylase/oxygenase; VIGS, virus-induced gene silencing; RT, reverse transcription; GFP, green fluorescent protein; RFP, red fluorescent protein; TMRM, tetramethylrhodamine methyl ester; aa, amino acid(s); MG, MitoTracker Green FM; c-IRS, cytosolic form of IleRS; DAPI, 4′,6-diamidino-2-phenylindole; cp-DNA, chloroplast DNA; TRV, tobacco rattle virus; PFGE, pulse-field gel electrophoresis.

date, there has been only one report regarding the function of an organelle-specific ARS (15). The insertion mutation of the organellar GlyRS gene was lethal, arresting embryo growth between the globular and heart stages of embryo development in *Arabidopsis*. An N-terminal fragment of the GlyRS protein was able to direct a marker protein into both chloroplasts and mitochondria (12). Thus, normal organellar ARS function is obviously essential for plant embryogenesis. However, there has been no report directly demonstrating how loss of organellar ARS function affects the development and physiology of chloroplasts and mitochondria, and how it in turn affects plant cells in which the organelles reside.

In this study, we investigated cellular functions of organellar ARSs by generating reduced-expression mutants using virus-induced gene silencing (VIGS), thereby circumventing the embryonic-lethal phenotypes associated with the complete loss of ARS function. VIGS of *NbERS* and *NbSRS*, encoding the *Nicotiana benthamiana* organellar forms of GluRS and SerRS, respectively, severely affected the numbers, morphology, and physiology of both chloroplasts and mitochondria. These data are consistent with the import of the *Arabidopsis* orthologs of NbERS and NbSRS into both chloroplasts and mitochondria and suggest that NbERS and NbSRS are responsible for the GluRS and SerRS activity required for translation in both organelles.

EXPERIMENTAL PROCEDURES

Virus-induced Gene Silencing—Various cDNA fragments of *NbERS* and *NbSRS* were PCR-amplified and cloned into the pTV00 vector containing a part of the TRV genome (16) using BamHI and ApaI sites. VIGS was carried out as described (16–18). The fourth leaf above the infiltrated leaf was used for RT-PCR and cytological analyses.

RT-PCR—Semiquantitative RT-PCR was performed with 5 μg of total RNA, isolated from the fourth leaf above the infiltrated leaf, as described previously (17). To detect the *NbERS* transcripts, the ERS-A (5′-ATGCCTCACTTTGCGCAT-3′ and 5′-TGCATCCTTCCACCTTTC-3′) and the ERS-B (5′-GTACCTCAAGCTGGGTTT-3′ and 5′-GCAAGTGGCAGTAAGATA-3′) primer sets were used. To detect the *NbSRS* transcripts, the SRS-A (5′-ACAGCTTATCAAAGCCGT-3′ and 5′-TAAACGTCTGTCCCATGT-3′) and the SRS-B (5′-ATGTTCATACTGTGCCGA-3′ and 5′-ATTGCTGACCTCACCATA-3′) primer sets were used. To detect the *NbIRS* transcripts, the IRS-A (5′-GGCAGTAAACCGCATTTC-3′ and 5′-CAACCCCCTTTCATCCAT-3′) and IRS-B (5′-ATCTCAGGTGGAGATTCT-3′ and 5′-CATTGTGCTATAGCCTCT-3′) primer sets were used. The primers used to detect nuclear genes were: for *rbcS*, 5′-CCTTGACATCACTTCCATT-3′ and 5′-AGCCCTCTGGCTTGTAGG-3′; for *Lhcb*, 5′-TGAAGGATATAGGGTTGGTG-3′ and 5′-GGGTCATTAATCTGGTCAAA-3′; for *FtsZ*, 5′-TCTGCTGCCTGTTCCCCCAA-3′ and 5′-AGCAACTCTGGACCCTCTCA-3′; for chalcone synthase (*CHS*), 5′-GAATACATGGCTCCTTCT-3′ and 5′-CCCAGGCCCAAATCCAAA-3′; for *ChlD*, 5′-TTGGACGTATCATGATTGTTGC-3′ and 5′-CTATGACGAGGAGAGACATTCC-3′; for *ChlH*, 5′-CACCCTTTGGCTCCTTGTATGT-3′ and 5′-CCATGATCACAGCCACATAGTG-3′; for *SGT*, 5′-AGAACGCTGAGCTTTTCG-3′ and 5′-CAGCAGATCCTTGATAGG-3′; for *SKP*, 5′-GTAGAAGAGTCAGTTGCC-3′ and 5′-TCAGCAGACTATTGACGC-3′; for pyruvate dehydrogenase E1α (*PDHE-1*α), 5′-GGGTCATGGGATTGTTGG-3′ and 5′-GCAGGATCAGACATGGAG-3′; for malate dehydrogenase (*MDH*), 5′-ACCCCTGGTGTTGCCGCT-3′ and 5′-CCATCTTGGGTTCGCTTG-3′; for actin, 5′-GCCACACTGTCCCAATTTATGA-3′ and 5′-GAAGCCAAAATAGAACCTCCAA-3′.

Subcellular Localization of AtERS and AtSRS—The *AtERS* cDNA fragments corresponding to the N-terminal 70 amino acids (residues 1–70) and the full-length sequence of 570 amino acids (residues 1–570) were cloned into the 326-GFP (green fluorescent protein) plasmid (19) using BamHI sites to generate AtERS-GFP fusion proteins. The *AtSRS* cDNA fragments corresponding to the N-terminal 90 amino acids (residues 1–90) and the full-length sequence of 514 amino acids (residues 1–514) were cloned into the same vector for the AtSRS-GFP fusion proteins. The various GFP fusion constructs and the F_1ATPase-γ-RFP fusion construct were introduced into protoplasts prepared from *Arabidopsis* seedlings by polyethylene glycol-mediated transformation (19). Expression of the fusion constructs was monitored at 24 h after transformation by confocal laser scanning microscopy, as described previously (18).

Measurement of Chlorophyll Content—The fourth leaf above the infiltrated leaf was collected from the VIGS plants and boiled in 95% ethanol at 80 °C for 30 min to extract chlorophyll. Chlorophyll concentration per unit fresh weight was calculated as described before (20).

Analysis of Starch Content—Leaves were harvested from the VIGS lines at 20 days after infiltration, and bleached in 80% (v/v) ethanol. After rinsing with double-distilled water, the leaves were stained with Lugol's iodine staining reagent (Sigma) and briefly destained with water.

Histochemical Analyses—Tissue sectioning and microscopy were carried out as described previously (17), using the fourth leaf above the infiltrated leaf from the VIGS lines.

Confocal Laser Scanning Microscopy—For TMRM (tetramethylrhodamine methyl ester, Molecular Probes) staining of mitochondria, TMRM was added into the leaf protoplasts at the final concentration of 200 nM. After incubation for 1–2 min at 25 °C, protoplasts were transferred to wells on microscope slides and examined by confocal microscopy (Carl Zeiss LSM 510) with a BP560-615 (543 nm excitation, 560–615 nm emission) optical filter to visualize the red fluorescent probe. Quantitative images were captured, and data were analyzed using the LSM 510 software (version 2.8). Chlorophyll autofluorescence was observed using an LP650 (excitation 488 nm, emission 650 nm) optical filter. MitoTracker Green FM (Molecular Probes) staining of protoplasts and 4′,6-diamidino-2-phenylindole staining of chloroplasts were carried out, as described previously (18).

PFGE Analysis—Protoplasts were prepared from the fourth to sixth leaves above the infiltrated leaf of the VIGS lines and counted. Roughly equal numbers of protoplasts from the VIGS lines were embedded, and pulse-field gel electrophoresis was carried out as described (18, 21). The *rbcL* cDNA was used as a probe.

RESULTS

Virus-induced Gene Silencing of the NbERS and NbSRS Caused Severe Leaf-yellowing Phenotypes—Functional genomics has been carried out in *N. benthamiana* using TRV-based virus-induced gene silencing (VIGS) to assess functions of signaling genes and genes that likely cause embryo or seedling lethality when their expression is suppressed. VIGS is based on the phenomenon that gene expression is suppressed in a sequence-specific manner by infection with viral vectors carrying host genes (22) and has been proved to be a powerful tool to analyze embryo- or seedling-lethal genes (17, 18). Using a VIGS screen, we found that gene silencing of the *N. benthamiana NbERS* and *NbSRS* genes, encoding isoforms of GluRS and SerRS, respectively, causes severe leaf yellowing and abnormal leaf morphology, while maintaining almost normal plant growth.

The full-length *NbERS* cDNA was obtained by 5′-rapid amplification of cDNA ends. The full-length *NbSRS* cDNA was obtained by PCR

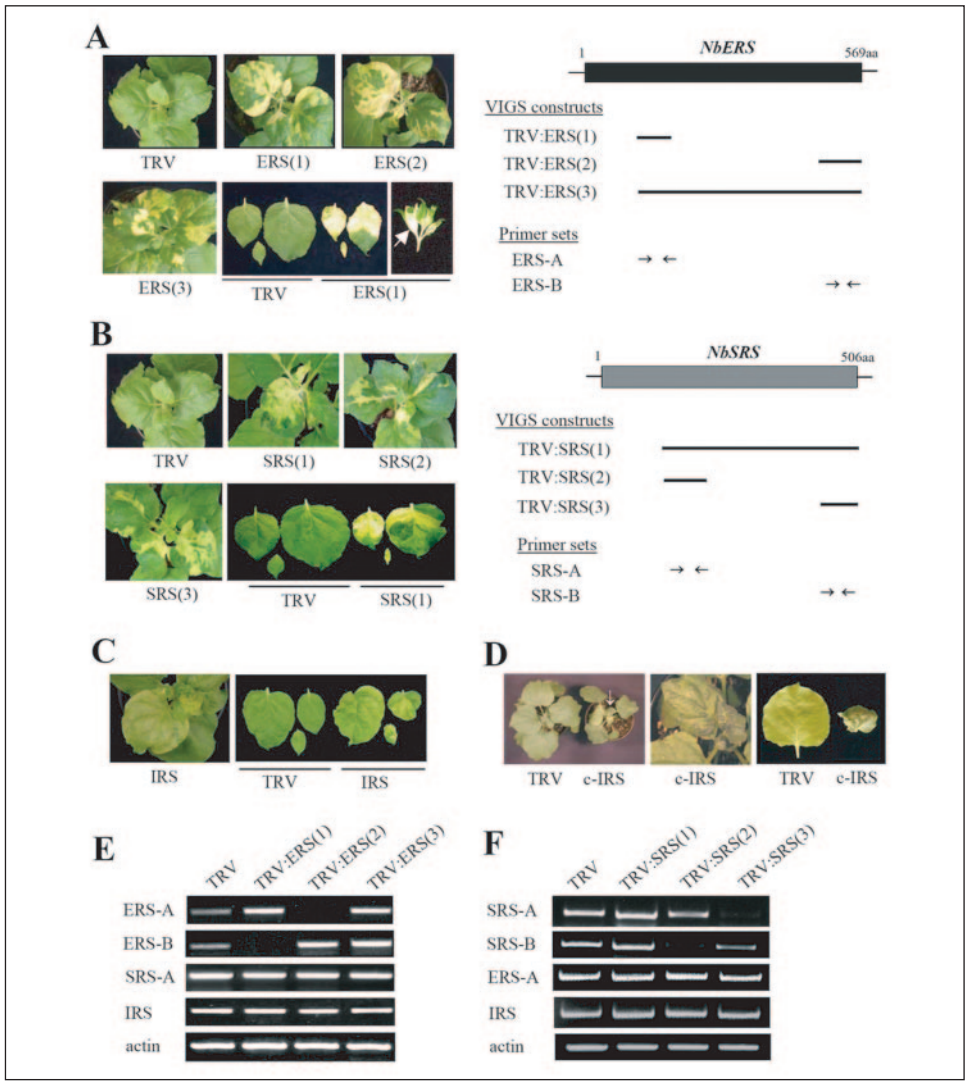

FIGURE 1. **VIGS phenotypes and suppression of endogenous transcripts.** *A*, schematic representation of the structure of *NbERS*, the cDNA regions used in the VIGS constructs, and the VIGS phenotypes of the three TRV:ERS VIGS lines. The *box* indicates the protein-coding region of *NbERS*. The three VIGS constructs containing different regions of the *NbERS* cDNA are marked by *bars*. *N. benthamiana* plants were infected with *Agrobacterium* containing the TRV control or one of the TRV:ERS constructs. The plants were photographed 20 days post-inoculation. The positions of the primer sets used for RT-PCR analyses, ERS-A and ERS-B, are also shown. The *arrow* indicates a flower bud with yellowed sepal. *B*, schematic representation of the structure of *NbSRS*, the cDNA regions used in the VIGS constructs, and the VIGS phenotypes of the three TRV:SRS VIGS lines. The plants were photographed 20 days post-inoculation. The positions of the primer sets, SRS-A and SRS-B, are shown. *C*, VIGS phenotypes of the TRV:IRS VIGS line. TRV:IRS construct contains a 1.5-kb cDNA fragment of *NbIRS* encoding the organellar IleRS. The plants were photographed 20 days post-inoculation. Note that VIGS of *NbIRS* caused only a weak leaf-yellowing phenotype. *D*, VIGS phenotypes of the TRV:c-IRS line. VIGS of the TRV:c-IRS construct containing a 0.3-kb cDNA fragment of the cytoplasmic IleRS resulted in arrested plant growth and abnormal leaf development in newly emerged leaves (*arrow*). *E*, semiquantitative RT-PCR analysis to examine the transcript levels of *NbERS*. RNA was extracted from the leaves of each VIGS line. As controls, *NbSRS*, *NbIRS*, and actin mRNA levels were examined. *F*, semiquantitative RT-PCR analysis to examine the transcript levels of *NbSRS*. As controls, *NbERS*, *NbIRS*, and actin mRNA levels were examined.

based on the sequence in the TIGR data base (accession number TC8134). *NbERS* and *NbSRS* encode polypeptides of 569 and 506 amino acids, respectively, corresponding to theoretical molecular masses of 63410.40 and 56266.37 Da. The *NbERS* and *NbSRS* genes exhibited high sequence similarity to the corresponding genes of prokaryotes, particularly cyanobacterial species, indicating that they encode an organellar isoform of GluRS and SerRS. The *Arabidopsis* data base contains one sequence encoding an organellar GluRS (GenBank^{TM} accession number NP_201210), designated *AtERS*, and a sequence for an organellar SerRS (AAL16281), designated *AtSRS*. When the amino acid sequences of the organellar *ERS* and *SRS* genes from plants were aligned with the corresponding genes from prokaryotes, a notable difference between the plant proteins and the corresponding bacterial proteins is that plant proteins contain a long extension at their N terminus, which has features of chloroplast and mitochondria targeting signals (23).

Suppression of the NbERS and NbSRS Transcripts by VIGS—To induce gene silencing of *NbERS* and *NbSRS*, we cloned different fragments of the *NbERS* and *NbSRS* cDNAs into the TRV-based VIGS vector pTV00 (16), and infiltrated *N. benthamiana* plants with *Agrobacterium* containing each plasmid (Fig. 1, *A* and *B*). TRV:ERS(1) and TRV:ERS(2) contain the N-terminal 333 bp and the C-terminal 383 bp of the *NbERS* cDNA, respectively, whereas TRV:ERS(3) contains a 1.5-kb cDNA fragment. Similarly, TRV:SRS(2) and TRV:SRS(3) contains the N-terminal 330 bp and the C-terminal 373 bp of the *NbSRS* cDNA, respectively, whereas TRV:SRS(1) contains a 1.2-kb cDNA fragment. VIGS with these constructs all resulted in a similar yellowing phenotype in newly emerged leaves, whereas overall plant growth was normal (Fig. 1, *A* and *B*). During flower formation, the sepals became yellow in the ERS plants (Fig. 1*A*). However, except that, flower development was normal in both ERS and SRS VIGS lines (data not shown). In contrast, VIGS of *NbIRS*, which encodes an organellar form of IleRS resulted in only a mild leaf-yellowing phenotype, when a 1.5-kb cDNA fragment was used for VIGS (Fig. 1*C*). As a control, we also carried out VIGS of *c-IRS*, which encodes a cytosolic form of IleRS, and it resulted in arrested plant growth and severe developmental abnormalities in newly emerged leaves, distinct from the VIGS phenotypes of the organellar ARSs (Fig. 1*D*).

Effects of gene silencing on the amounts of endogenous *NbERS* and *NbSRS* mRNAs were examined by semiquantitative RT-PCR (Fig. 1, *E* and *F*). RT-PCR using the ERS-A primers (indicated in Fig. 1*A*) produced significantly reduced amounts of PCR products in the yellow sectors of the leaves from the TRV:ERS(2) line, indicating that the endogenous level of the *NbERS* transcripts is greatly reduced in these plants (Fig. 1*E*). The same primers detected high levels of viral genomic transcripts containing the N-terminal region of *NbERS* in the TRV:ERS(1) and TRV:ERS(3) lines. Similarly, RT-PCR using the ERS-B prim-

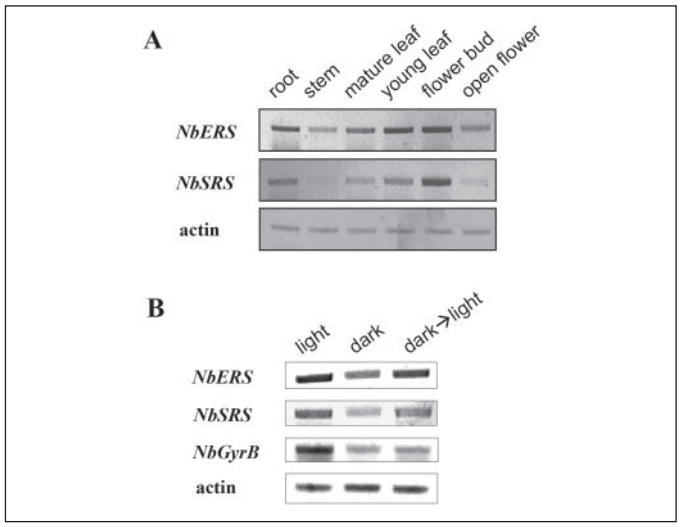

FIGURE 2. **Expression of the *NbERS* and *NbSRS* genes.** Semiquantitative RT-PCR analysis was carried out with total RNA from *N. benthamiana* plants using the *NbERS*- and *NbSRS*-specific primers. As a control, the transcript level of actin was examined. *A*, expression in various plant tissues. *B*, light-stimulated expression. Seedlings were grown for 7 days under normal light conditions (16 h light/8 h dark) (*light*), under dark conditions (*dark*), or under dark conditions followed by a transfer to light for 1 h (*dark→light*). As a control for light regulation, the expression of *NbGyrB*, which encodes the chloroplast-targeted DNA gyrase subunit B (18) was examined.

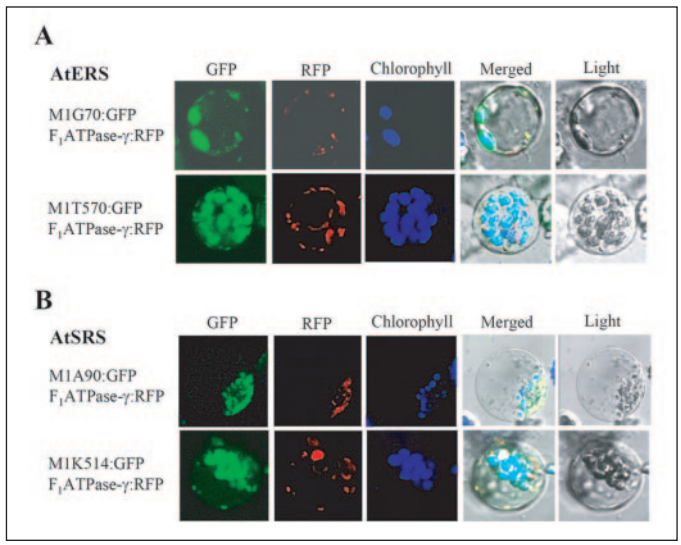

FIGURE 3. **Targeting of AtERS and AtSRS to both chloroplasts and mitochondria.** *Arabidopsis* protoplasts were cotransformed with GFP fusion constructs of AtERS or AtSRS and the F_1ATPase-γ-RFP construct, and the localization of the fluorescent signals was examined at 24 h after transformation using a confocal laser scanning microscope. Chloroplasts and mitochondria were visualized by chlorophyll autofluorescence and the red fluorescence of F_1ATPase-γ-RFP, respectively. Chlorophyll autofluorescence is pseudo-colored (*blue*) to distinguish it from the red fluorescence of RFP. Merged and bright-field images are also shown. *A*, GFP was fused to the N-terminal 70-aa peptide of AtERS in M1G70:GFP, and to the full-length AtERS in M1T570:GFP. *B*, GFP was fused to the N-terminal 90-aa peptide of AtSRS in M1A90:GFP, and to the full-length AtSRS in M1K514:GFP.

ers (indicated in Fig. 1*A*) produced significantly reduced amounts of PCR products in the yellow sectors of leaves from the TRV:ERS(1) line, whereas the same primers detected high levels of viral genomic transcripts containing the C-terminal region of *NbERS* in the TRV:ERS(2) and TRV:ERS(3) lines. In all of the ERS VIGS lines, the transcript level of *NbSRS*, *NbIRS*, and actin remained constant (Fig. 1*E*).

Silencing of *NbSRS* was also examined by semiquantitative RT-PCR (Fig. 1*F*). RT-PCR using the SRS-A and SRS-B primers produced significantly reduced amounts of PCR products in yellow sectors of leaves from the TRV:SRS(3) and TRV:SRS(2) lines, respectively, indicating that the endogenous level of the *NbSRS* transcripts is significantly reduced in those plants. In all of the SRS VIGS lines, the transcript levels of *NbERS*, *NbIRS*, and actin stayed constant (Fig. 1*F*). These results clearly show that VIGS using the *NbERS* and *NbSRS* cDNA fragments specifically suppresses expression of these genes. The transcripts levels of *NbERS* and *NbSRS* in TRV were identical to those in wild-type, indicating that TRV infection did not affect the expression of *NbERS* and *NbSRS* (supplementary Fig. S1*A*). Although VIGS of *NbIRS* caused only mild phenotypes compared with silencing of *NbERS* and *NbSRS*, the degree of gene silencing of *NbIRS* in its VIGS lines was similar to that of *NbERS* and *NbSRS*, at least at the mRNA level (supplementary Fig. S1*B*). These data suggest that each organellar ARS may have a distinct threshold level required for normal organelle function.

Expression Patterns of NbERS and NbSRS—To examine tissue-specific expression patterns of *NbERS* and *NbSRS*, semiquantitative RT-PCR analyses were carried out using the *NbERS*- and *NbSRS*-specific primer sets. RT-PCR products of *NbERS* and *NbSRS* were detected in all of the tissues examined, including roots, stems, mature leaves, young leaves, flower buds, and open flowers in *N. benthamiana*, with somewhat higher levels of the transcripts in young tissues such as young leaves and flower buds (Fig. 2*A*). The light-dependent gene expression of *NbERS* and *NbSRS* was examined by semiquantitative RT-PCR (Fig. 2*B*). *N. benthamiana* seedlings were grown for 7 days on MS media under normal light conditions (16 h light/8 h dark), under dark conditions, or under dark conditions followed by a transfer to light for 1 h. The *NbERS* and *NbSRS* mRNA levels were lower in dark-grown seedlings than light-grown seedlings, but exposure to light for 1 h after the dark-grown period increased the *NbERS* and *NbSRS* mRNA levels to that of light-grown seedlings (Fig. 2*B*). As a positive control, *NbGyrB* expression in response to light was also monitored. *NbGyrB* encodes subunit B of DNA gyrase, which plays a critical role in chloroplast DNA metabolism, and is induced by light (18). These results indicate that expression of *NbERS* and *NbSRS* is stimulated by light.

Dual Targeting of AtERS and AtSRS to Chloroplasts and Mitochondria—We examined the subcellular localization of AtERS and AtSRS (Fig. 3). Both AtERS and AtSRS contain a long extension at their N terminus, which contains features of dual targeting signals to chloroplasts and mitochondria (23). We generated fusion proteins in which the N-terminal regions or the full-length proteins of AtERS and AtSRS were fused to GFP. For AtERS, the N-terminal sequence of 70 aa (Met-1 to Gly-70, M1G70) and the full-length sequence of 570 aa (Met-1 to Thr-570, M1T570) were used. For AtSRS, the N-terminal sequence of 90 aa (Met-1 to Ala-90, M1A90) and the full-length sequence of 514 aa (Met-1 to Lys-514, M1K514) were used. These DNA constructs encoding different forms of AtERS-GFP or AtSRS-GFP fusion proteins under the control of the CaMV35S promoter were introduced into protoplasts isolated from *Arabidopsis* seedlings. To track mitochondria, a DNA construct encoding an F_1ATPase-γ-RFP fusion protein of the mitochondrial F_1ATPase-γ subunit (19), and red fluorescent protein (RFP) was cotransformed into the protoplasts. After incubation at 25 °C for 24 h, expression of the introduced genes was examined by confocal laser scanning microscopy with different filters to capture images of GFP, RFP, and autofluorescence of chlorophyll.

For both AtERS(M1G70)-GFP- and AtERS(M1T570)-GFP-transformed protoplasts, the green fluorescent signal completely overlapped with both autofluorescence of chloroplasts and the red fluorescent signal of F_1ATPase-γ-RFP, indicating that the AtERS protein was targeted to both chloroplasts and mitochondria (Fig. 3*A*). Similarly, both AtSRS(M1A90)-GFP- and AtSRS(M1K514)-GFP-transformed protoplasts exhibited overlapping fluorescent signals from GFP, RFP, and

chlorophyll autofluorescence, indicating dual targeting of AtSRS (Fig. 3*B*). These results demonstrate that the N-terminal extension of AtERS and AtSRS contains a signal for transport of the protein to both chloroplasts and mitochondria.

Numbers of Chloroplasts and Mitochondria—Protoplasts were generated from yellow sectors of the leaves from the TRV:ERS and TRV:SRS lines, and examined by confocal laser scanning microscopy (Fig. 4*A*). As controls, protoplasts from the TRV were also observed. In both TRV:ERS and TRV:SRS, almost all of the protoplasts, mostly originated from leaf mesophyll cells, exhibited drastically reduced numbers of chloroplasts. The average number of chloroplasts in the TRV:ERS and TRV:SRS lines was about 27 and 35% of the TRV control, respectively (Fig. 4*B*). Chlorophyll content of the leaves was consistently much lower in the VIGS lines than the TRV controls (Fig. 4, *C* and *G*). Furthermore, chloroplasts from the TRV:ERS and TRV:SRS lines were significantly smaller than TRV controls (Fig. 4*D*) and measured ~31 and 55% of the average control diameter, respectively. Some of the chloroplasts in the TRV:ERS and TRV:SRS lines were dumbbell-shaped, indicating disrupted chloroplast division (results not shown). The chloroplast numbers and diameter, chlorophyll autofluorescence, and total chlorophyll contents in TRV were very similar to those in wild-type (supplementary Fig. 2, *A*–*D*).

Mitochondria in leaf protoplasts isolated from the TRV control, TRV:ERS, and TRV:SRS lines were examined by TMRM and MitoTracker Green FM (MG) fluorescent probes (Fig. 4, *A*, *E*, and *F*). TMRM is a lipophilic cation that accumulates in mitochondria in proportion to the mitochondrial membrane potential (24), and a drop in the membrane potential leads to a decrease in fluorescence. The average TMRM fluorescence of protoplasts from TRV:ERS and TRV:SRS leaves was ~9 and 25% of TRV controls, respectively (Fig. 4*E*). This decrease in fluorescence could be due to either reduced mitochondrial numbers or altered membrane potential of mitochondria in the protoplasts. MitoTracker Green FM (MG) accumulates in mitochondria regardless of the mitochondrial membrane potential, and is widely used to determine mitochondrial mass (25). The MG fluorescence of the protoplasts from TRV:ERS and TRV:SRS leaves, ~8 and 11%, respectively, was significantly lower than that of the TRV control (Fig. 4, *A* and *F*). This indicates that mitochondrial numbers and/or mass are reduced in the ERS and SRS VIGS lines. The TMRM and MG fluorescence of mitochondria in TRV were very similar to those in wild-type (supplementary Fig. S2, *E* and *F*).

Ultrastructural Analysis of Chloroplasts—Transmission electron microscopy of transverse leaf sections of the TRV:ERS and TRV:SRS VIGS lines showed a large difference in the chloroplast number and morphology compared with TRV controls (Fig. 5), whereas the leaf cell structure was relatively normal (results not shown). In TRV controls, mesophyll cell chloroplasts have a well developed thylakoid membrane system and large starch granules (Fig. 5, *A*, *D*, and *G*). Yellow sectors of the leaves from the TRV:ERS and TRV:SRS lines exhibited severely reduced chloroplast numbers, and morphological abnormalities were apparent in the chloroplasts (Fig. 5, *B*, *E*, *C*, and *F*). The abnormal chloroplasts were small and irregular in shape, and contained few starch grains (Fig. 5, *E* and *F*). The thylakoid membranes were either poorly developed or in the process of disintegration and exhibited radical alterations in arrangement and distribution (Fig. 5, *H* and *I*). Interestingly, some of the chloroplasts in the TRV:ERS and TRV:SRS lines exhibited a dumbbell-shaped morphology with a central constriction, mimicking chloroplasts undergoing division, but with the two daughter chloroplasts differing in size (Fig. 5*F*). Those organelles may represent chloroplasts arrested during division due to abnormal conditions within the organelle. Consistent with the lack of starch accumulation in the abnormal chloroplasts (Fig. 5, *B* and *C*), starch contents in the yellowing leaves from the TRV:ERS and TRV:SRS lines were much lower than that of TRV leaves during the light period, based on iodine staining (Fig. 5*J*). As expected, the yellow sectors of the leaves from the TRV:ERS and TRV:SRS lines perfectly overlapped with the regions that were not stained with iodine (Fig. 5*J*, results not shown). In contrast to the leaf-yellowing phenotype of the organellar ARSs, VIGS of the cytosolic form of IleRS (c-IRS) resulted in arrested plant growth and abnormal leaf development (Fig. 1*D*). Transverse leaf sections revealed that the TRV control leaves had the typical leaf structure of dicotyledonous plants (Fig. 5*K*). In the TRV:c-IRS leaves, the cell numbers decreased, and the cell sizes increased in every layer, which was accompanied by an irregular cell morphology, whereas the typical dorsoventral organization of the palisade and mesophyll cells was mostly maintained (Fig. 5*L*). Transmission electron microscopy showed that chloroplasts of the mesophyll cells in the TRV:c-IRS lines contained large starch granules (Fig. 5*M*), a dramatic contrast to the lack of starch accumulation in the TRV:ERS and TRV:SRS chloroplasts (Fig. 5, *B* and *C*). Thus, depletion of the organellar or the cytosolic form of ARS resulted in completely different cellular and organellar phenotypes in plants.

Chloroplast DNA Structure—Isolated protoplasts from TRV, TRV:ERS, and TRV:SRS lines were stained with DAPI and squashed on a microslide to visualize individual chloroplasts and chloroplast nucleoids (Fig. 6*A*). The TRV control exhibited faint staining of chloroplast nucleoids. Chloroplast nucleoids are dispersed as small particles in the stroma mostly associated with thylakoids, and the nucleoid numbers and chloroplast DNA (cp-DNA) content vary during chloroplast development (26, 27). Recent studies have revealed that the amount of cp-DNA per chloroplast decreases as the chloroplasts develop, and reaches undetectable levels in mature leaves long before the onset of senescence in *Arabidopsis* and maize (28, 29). Compared with the TRV control, chloroplasts of TRV:ERS and TRV:SRS lines had increased DAPI fluorescence suggesting increased chloroplast DNA content, whereas the chloroplast size was much reduced.

We used PFGE to estimate the size of cp-DNA molecules in leaf chloroplasts isolated from TRV, TRV:ERS, and TRV:SRS VIGS lines (Fig. 6*B*). Equal numbers of leaf protoplasts prepared from each VIGS line were embedded and subjected to PFGE. Previously, Lilly *et al.* (21) demonstrated that both linear and circular DNA fibers with one to four copies of the chloroplast genome are present in tobacco chloroplasts, with monomers being the predominant structure. In the TRV control, hybridization of the *rbcL* gene probe to DNA blots from PFGE consistently revealed a band corresponding to the monomeric cp-DNA (Fig. 6*B*). Faint hybridization signals below the monomeric band (indicated by the *red arrow*) are likely to represent cp-DNA molecules of subgenomic size or sheared cp-DNA. In the TRV:ERS line, a distinct monomeric cp-DNA band was not detected and the subgenomic hybridization signal was prominent. In the TRV:SRS line, the monomeric band was visible, but the hybridization signal from the subgenomic cp-DNA was more prominent than control cp-DNA. The small cp-DNA molecules abundant in these lines could be a cleavage product of replication intermediates. In contrast, cp-DNA molecules containing multiple chloroplast genomes were not observed in these VIGS lines. Thus, compromised translation activity in the chloroplasts appeared to induce accumulation of cp-DNA representing partial genome units.

Expression of the Nuclear Genes for the Chloroplast- or Mitochondria-targeted Proteins, and the Chlorophyll Biosynthetic Enzymes—Chloroplast development involves coordinated expression of both plastidic and nuclear genes, and subsequent translocation of nuclear-encoded proteins into developing chloroplasts (30). It has been proposed that

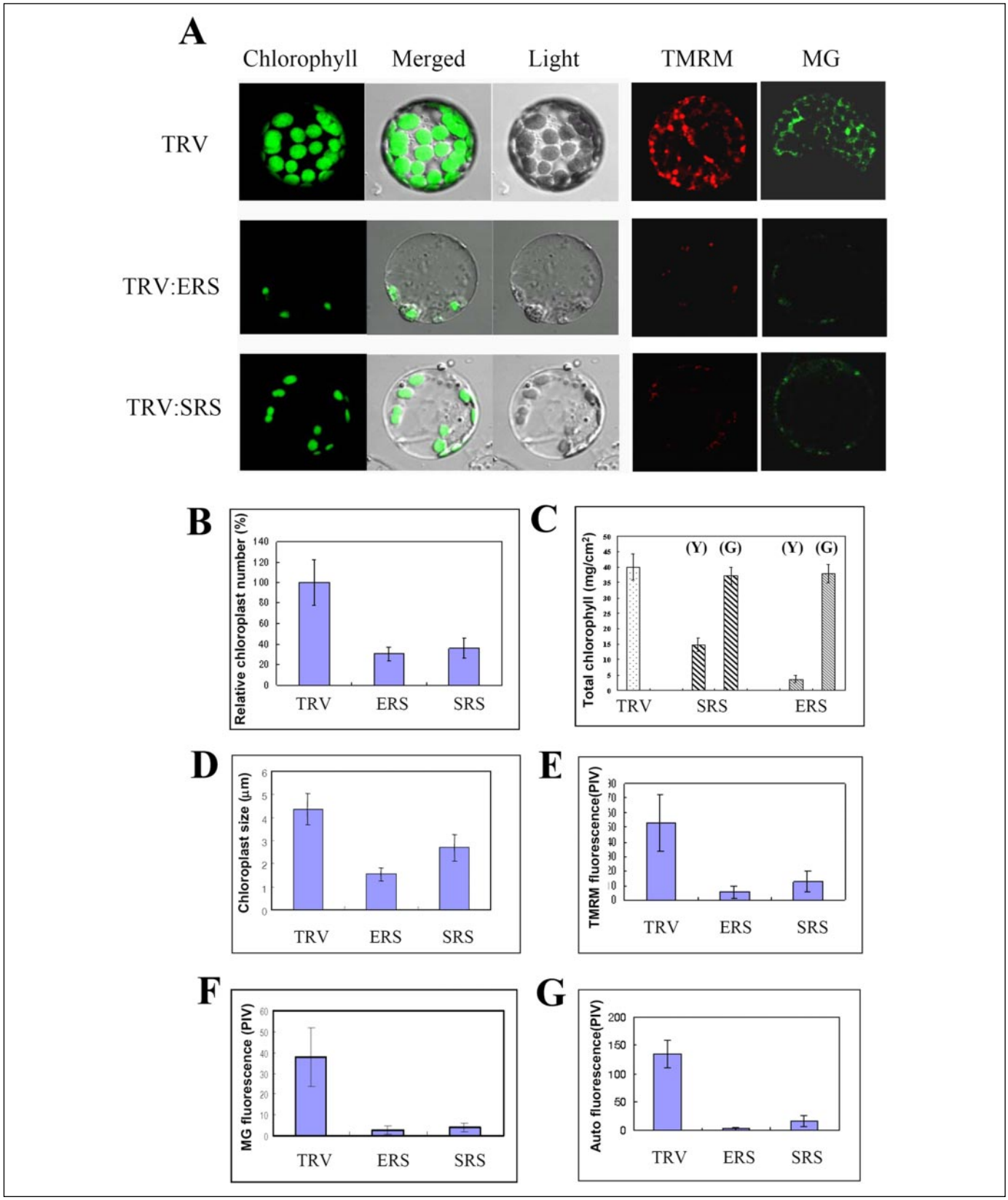

FIGURE 4. **Numbers of chloroplasts and mitochondria.** *A*, confocal laser scanning microscopy of chloroplasts and mitochondria in protoplasts isolated from the TRV, TRV:ERS, and TRV:SRS VIGS lines. Chloroplasts were visualized by chlorophyll autofluorescence (*red fluorescence*), and mitochondria were visualized by staining with TMRM and MitoTracker Green FM (*MG*). Bright-field and merged images are shown. *B*, confocal microscopy was used to determine the number of chloroplasts per protoplast. TRV controls had, on average, 57 chloroplasts per protoplast. The data points represent means ± S.D. of 40–50 individual protoplasts. *C*, total chlorophyll contents in the yellow (*Y*) and green (*G*) sectors of the leaves from VIGS lines were measured, as described (20). *D*, the average diameter of chloroplasts was measured. The data points represent means ± S.D. of 40–50 individual protoplasts. *E–G*, the average fluorescence of TMRM (*E*), MitoTracker Green FM (*F*), and chlorophyll autofluorescence (*G*) in individual protoplasts was quantified by confocal microscopy. Data points represent means ± S.D. of 40–50 individual protoplasts. *PIV*, pixel intensity values.

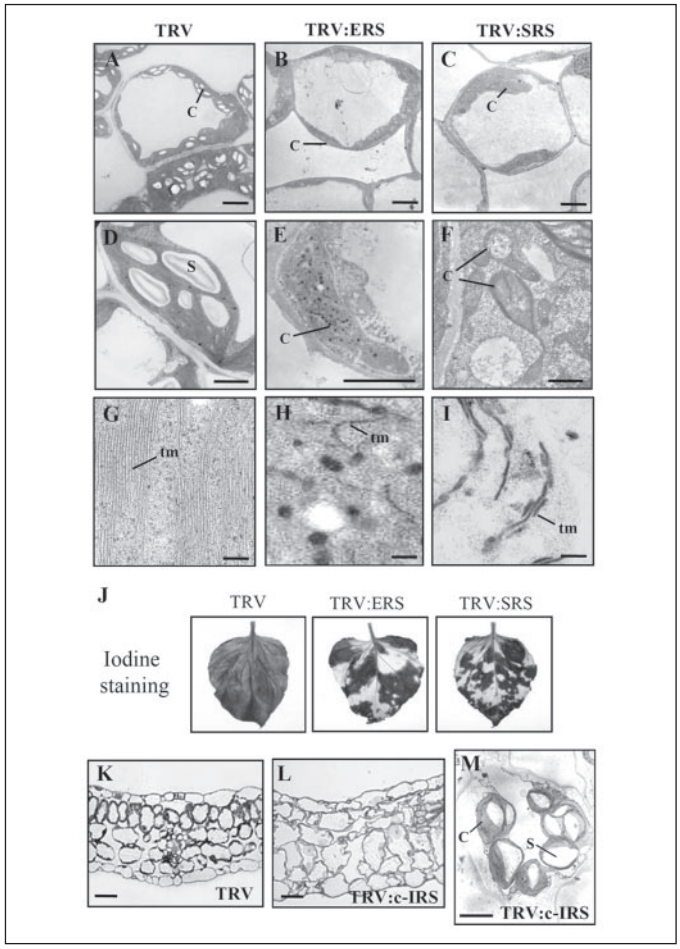

FIGURE 5. **Ultrastructural analysis of mesophyll cell chloroplasts and mitochondria.** *A–I*, transmission electron micrographs of leaf mesophyll cells (*A–C*), chloroplasts (*D–F*), and chloroplast thylakoid membranes (*G–I*) of the TRV control (*A*, *D*, and *G*), TRV:ERS (*B*, *E*, and *H*), and TRV:SRS (*C*, *F*, and *I*) lines. *c*, chloroplast; *s*, starch; *tm*, thylakoid membrane. *Scale bars* = 5 μm in *A–C*; 1 μm in *D–F*; 0.1 μm in *G–I*. *J*, iodine staining of the leaves from the TRV, TRV:ERS, and TRV:SRS lines. Black staining indicates accumulated starch. *K–M*, light micrographs of leaf transverse sections of the TRV (*K*) and TRV:c-IRS (*L*) lines, and transmission electron micrograph of a mesophyll cell of the TRV:c-IRS (*M*) line. *c*, chloroplast; *s*, starch. *Scale bars* = 100 μm in *K* and *L*; 10 μm in *M*.

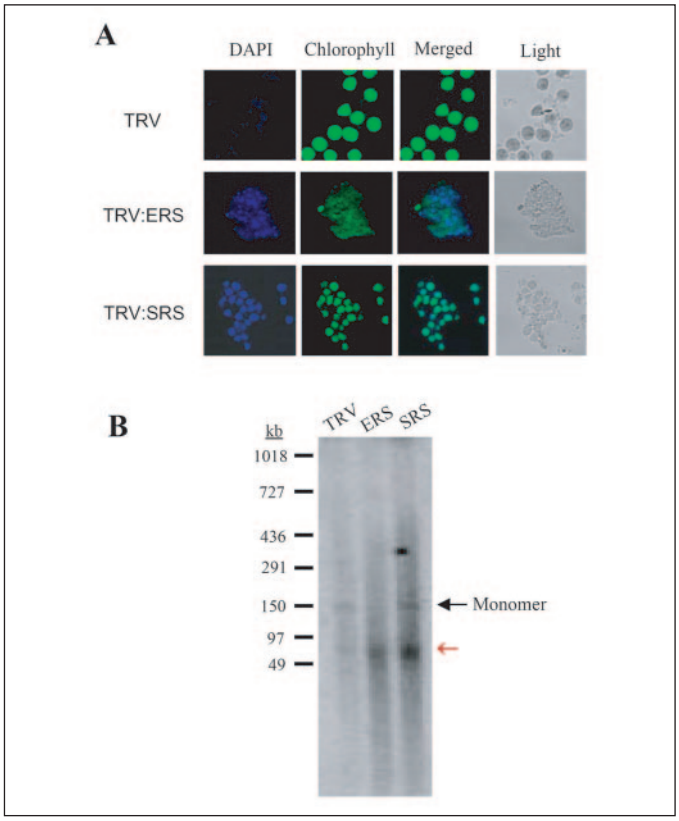

FIGURE 6. **DAPI staining and PFGE analysis of chloroplast DNA.** *A*, DAPI staining of chloroplast DNA (cp-DNA). Protoplasts were isolated from the fourth leaf above the infiltrated leaf in TRV, TRV:ERS, and TRV:SRS VIGS lines. After DAPI staining, the protoplasts were gently squashed under a microslide to visualize individual chloroplasts. Fluorescent signals of DAPI and chlorophyll autofluorescence were examined using a confocal laser scanning microscope. *B*, pulse-field gel electrophoresis of cp-DNA was carried out, as described previously (21). The DNA blots were hybridized with a radiolabeled *rbcL* gene probe. The *black arrow* indicates the band representing monomeric molecules of cp-DNA, and the *red arrow* indicates subgenomic sized or sheared cp-DNA. DNA size markers are indicated in kilobases.

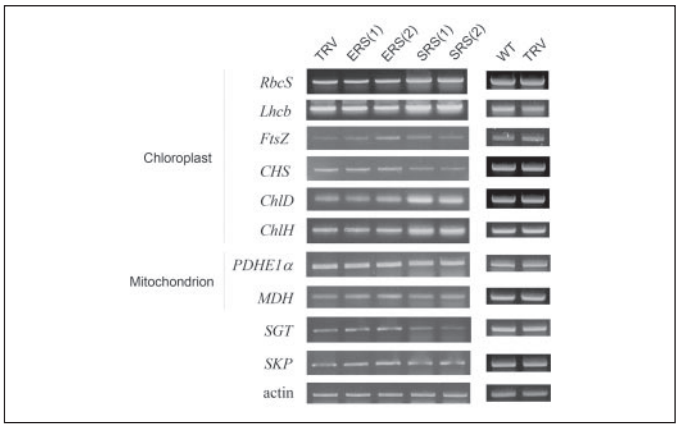

FIGURE 7. **Expression of the nuclear genes coding for chloroplast- or mitochondria-targeted proteins, and chlorophyll biosynthetic enzymes.** Semiquantitative RT-PCR analysis was carried out with total RNA from wild-type, TRV, and two different TRV:ERS and TRV:SRS lines. As controls, the transcript levels of *SGT*, *SKP*, and actin were examined.

signals from chloroplasts, known as plastid factors, regulate nuclear gene expression (31). The effects of depletion of the organellar ARSs on transcription of various nuclear genes were examined by semiquantitative RT-PCR using RNA from wild-type and TRV leaves, and yellow sectors of the TRV:ERS and TRV:SRS leaves (Fig. 7). The mRNA levels of nuclear genes encoding chloroplast-targeted proteins such as RbcS (Rubisco small subunit), Lhcb (chlorophyll a/b-binding protein), and FtsZ (chloroplast division protein) in the TRV:ERS and TRV:SRS lines were very similar to those in the TRV control. Furthermore, transcript levels of nuclear genes that encode enzymes in the chlorophyll biosynthesis pathway, such as ChlD, ChlH, and CHS (chalcone synthase), in the TRV:ERS and TRV:SRS lines were also similar to those of TRV (Fig. 7). As controls, expression of *SGT1* and *SKP1*, signaling genes in plant defense (32–34), and the actin gene remained constant. Thus, many nuclear genes for chloroplast function were expressed at normal levels, regardless of the grossly abnormal status of chloroplasts in the cell, indicating disrupted communication between the chloroplasts and the nucleus. This result indicates that the chloroplast translation system may be involved in biosynthesis of the plastid factor.

We also observed that expression of nuclear genes encoding the mitochondrial pyruvate dehydrogenase E1α (*PDHE1*α) and malate dehydrogenase (*MDH*) remained unaffected by impaired mitochondrial function in the leaf cells of the ERS and SRS VIGS plants (Fig. 7). The mechanism of communication between mitochondria and the nucleus has been well documented in yeast and animal systems (35, 36). However, the regulation of nuclear-encoded mitochondrial proteins in plants is largely unknown. The results in this study suggest that a defec-

tive mitochondrial translation system may inhibit the signaling of mitochondrial dysfunction to the nucleus.

DISCUSSION

In this study, we show that depletion of the organellar forms of glutamyl-tRNA synthetase (NbERS) and seryl-tRNA synthetase (NbSRS) effectively eliminated both chloroplasts and mitochondria, indicating that these proteins are responsible for the GluRS and SerRS activity required for translation in chloroplasts and mitochondria. In higher plants, cytosolic tRNAs are all nucleus-encoded, and chloroplastic tRNAs are all chloroplast-encoded (37). However, the mitochondrial genome specifies fewer than the minimally required tRNAs, and as a result, one-third to one-half of the mitochondrial tRNAs are nuclear-encoded and imported from the cytosol (38, 39). The number of imported tRNAs and their identities vary among plant species, and in *Arabidopsis*, these include $tRNA^{Ala}$, $tRNA^{Thr}$, $tRNA^{Val}$, and $tRNA^{Gly}$ (38, 39). To complicate matters, some of the mitochondria-encoded tRNA genes, such as *trnW* in *Arabidopsis* (40), and *trnP* and *trnR* in rice (41), are either untranscribed or processed inefficiently. In *Arabidopsis*, the cytosolic $tRNA^{Trp}$ is imported to mitochondria to compensate for the lack of expression of the *trnW* gene (40). Correlated with import of the cytosolic tRNAs into mitochondria, the cytosolic forms of some ARSs, such as AlaRS, ThrRS, ValRS, and GlyRS in *Arabidopsis*, are imported into the mitochondria to catalyze aminoacylation of their cognate nucleus-encoded tRNAs (38). For *Arabidopsis* AlaRS, ThrRS, ValRS, and GlyRS, a single gene encodes both the cytosolic and mitochondrial enzymes by using two in-frame translation initiation codons (7, 8). However, further studies revealed that the mitochondria-targeted cytosolic GlyRS is inactive in the mitochondrial fraction, and the organellar GlyRS is likely to glycylate both the organelle-encoded $tRNA^{Gly}$ and the imported $tRNA^{Gly}$ (12). Thus, to understand the complete picture of mitochondrial import of individual tRNAs and ARS enzymes in plants, further investigation is required.

The mitochondrial genome of *Nicotiana tabacum*, a close relative of *N. benthamiana*, was recently sequenced (42) and found to contain a single chloroplast-derived gene for $tRNA^{Glu}$ (*trnE-UUC*) and three native genes for $tRNA^{Ser}$ (*trnS-GCU*, *trnS-UGA*, and *trnS-GGA*). These genes have also been found in the mitochondrial genome of *Arabidopsis*, rapeseed, wheat, rice, and sugar beet (39, 43–46). In these plants, and most likely in *N. benthamiana* as well, the mitochondria-encoded tRNAs are sufficient to read all the codons of glutamic acid and serine by wobble base pairing for protein synthesis in mitochondria. Consistently, the cytosolic forms of *Arabidopsis* GluRS and SerRS do not have the conserved mitochondria-targeting signal or the two different translation initiation codons at the N terminus (data not shown). Furthermore, expression of the maize organellar SerRS complemented the phenotype of a yeast mutant with a defective mitochondrial SerRS, and the purified organellar SerRS protein aminoacylated the maize chloroplast and mitochondrial $tRNA^{Ser}$ with equal efficiency (47). These results, together with our current results, suggest that the organellar forms of GluRS and SerRS are responsible for aminoacylation of $tRNAs^{Glu}$ and $tRNAs^{Ser}$ in the mitochondria of higher plants.

The numbers of chloroplasts are much reduced in affected cells of the ERS and SRS VIGS lines. Furthermore, the chloroplasts were significantly smaller than those of the TRV control (approximately one-thirtieth and one-sixth the control volume, for ERS and SRS, respectively), but had a higher cp-DNA content. In higher plants, the population size of mature chloroplasts and photosynthetic competence are achieved by the post-mitotic division of young chloroplasts in the expanding mesophyll cells (48, 49). At early stages, the proplastids in mitotic cells undergo a series of divisions that are correlated with cell division, ensuring that the young post-mitotic cells contain at least 15 proplastids (48, 49). During cell expansion, the young chloroplasts expand and begin to divide when they have grown to ~50% of their final volume. The reduced sizes and numbers of chloroplasts in the ERS and SRS VIGS lines indicate defective proplastid/chloroplast expansion and division. The chloroplasts in the ERS and SRS VIGS lines also appeared to accumulate a large number of small-sized cp-DNA molecules representing partial genome units (Fig. 6*B*). The abnormal cp-DNA structure as well as other defects in biogenesis due to suppression of plastid translation likely inhibited further growth and differentiation of chloroplasts and suppressed normal division, which eventually led to degeneration of the organelle.

The ERS, SRS, and IRS VIGS lines each showed a different degree of phenotypic severity. Suppression of *NbERS* resulted in the most severe abnormality among the three genes, as shown by chloroplast numbers and leaf chlorophyll content, whereas gene silencing of *NbIRS* caused only mild leaf yellowing. In the *NbERS*, *NbSRS*, and *NbIRS* VIGS lines, the degree of silencing of each individual mRNA did not seem to differ significantly (Fig. 1 and Supplementary Fig. S1). A possible reason for the difference in phenotypes may be differences in the threshold level of each ARS required for minimal translation activity to maintain normal chloroplast function. Threshold differences may reflect differences in biochemical characteristics of individual ARS proteins or substrate availability for each ARS within the chloroplasts. Recently, in addition to the role in the translation process, ARSs have been shown to have other cellular functions, including RNA processing and trafficking, apoptosis, rRNA synthesis, angiogenesis, and inflammation (50, 51). In plants, it has been reported that the plastid-encoded $tRNA^{Glu}$ mediates the switch in RNA polymerase usage from nuclear-encoded plastid RNA polymerase to plastid-encoded plastid RNA polymerase during chloroplast biogenesis, by directly binding to nuclear-encoded plastid RNA polymerase and inhibiting the transcriptional activity of nuclear-encoded plastid RNA polymerase (52). Thus, there is a possibility that the phenotypic differences we observed in this study are caused by other functions of the organellar ARSs, yet unidentified.

Biogenesis of plastids is tightly coupled to temporal and spatial stages of plant development and involves coordinated expression of plastidic genes and nuclear genes encoding chloroplast proteins, which requires precise communication between the nucleus and plastids. Signals from the plastid, termed "plastid factors," have been postulated to provide the nuclear genome with information about the developmental status of the plastid (31). These signals were initially identified by their capacity to affect transcription of subsets of nuclear genes. For example, impaired chloroplast function or development by herbicides or mutations resulted in reduced expression of the nuclear genes *Lhcb* (chlorophyll a/b-binding protein) and *RbcS* (Rubisco small subunit) (53–55). Recent evidence suggests that at least two different plastid factors operate in plants: redox signals (56) and intermediates in chlorophyll biosynthesis (57, 58). Recently, Ahlert *et al.* (59) used cell-line specific recombination-based knockouts of chloroplast translation to demonstrate that plastid protein synthesis is essential for plant development and cell division. Furthermore, the nuclear-encoded plastid ribosomal proteins L35 and S9 were shown to be critical for the very early stages of embryo development in maize (60, 61).

These results indicate that the chloroplast gene(s) and gene product(s) critically influence processes outside the chloroplast, in addition to the well established metabolic signals between the chloroplast and nucleus. In this study, we observed that the defective chloroplasts that result from depletion of GluRS and SerRS did not influence the expres-

sion of diverse nuclear genes encoding chloroplast-targeted photosynthetic proteins and chlorophyll biosynthesis enzymes. Thus, in the affected cells, the nucleus did not seem to sense the functional status of the chloroplasts. We speculate that a block of protein synthesis within the plastids resulting from a lack of GluRS and SerRS activity may interfere with the biosynthetic pathway of the plastid factors. Genetic analyses of plastid-encoded genes may identify the pathway and the signaling mechanism that links the plastids to the nucleus.

Acknowledgments—We thank Dr. Zee Won Lee (Korea Basic Science Institute, Taejon, Korea) for technical help with confocal laser scanning microscopy.

REFERENCES

1. Ibba, M., and Soll, D. (2000) *Annu. Rev. Biochem.* **69,** 617–650
2. Ribas de Pouplana, L., and Schimmel, P. (2001) *Trends Biochem. Sci.* **26,** 591–596
3. Browning, K. S. (1996) *Plant Mol. Biol.* **32,** 107–144
4. Steimetz, A., and Weil, J. H. (1986) *Methods Enzymol.* **118,** 212–231
5. Small, I., Akashi, K., Chapron, A., Dietrich, A., Duchene, A. M., Lancelin, D., Maréchal-Drouard, L., Menad, B., Mireau, H., Moudden, Y., Ovesna, J., Peeters, N., Sakamoto, W., Souciet, G., and Wintz, H. (1999) *J. Hered.* **90,** 333–337
6. Guillemaut, P., Steinmetz, A., Burkard, G., and Weil, J. H. (1975) *Biochim. Biophys. Acta* **378,** 64–72
7. Mireau, H., Lancelin, D., and Small, I. D. (1996) *Plant Cell* **8,** 1027–1039
8. Souciet, G., Menand, B., Ovesna, J., Cosset, A., Dietrich, A., and Wintz, H. (1999) *Eur. J. Biochem.* **266,** 848–854
9. Akashi, K., Grandjean, O., and Small, I. (1998) *FEBS Lett.* **431,** 39–44
10. Peeters, N. M., Chapron, A., Giritch, A., Grandjean, O., Lancelin, D., Lhomme, T., Vivrel, A., and Small, I. (2000) *J. Mol. Evol.* **50,** 413–423
11. Menand, B., Maréchal-Drouard, L., Sakamoto, W., Dietrich, A., and Wintz, H. (1998) *Proc. Natl. Acad. Sci. U. S. A.* **95,** 11014–11019
12. Duchene, A.-M., Peeters, N., Dietrich, A., Cosset, A., Small I. D., and Wintz, H. (2001) *J. Biol. Chem.* **276,** 15275–15283
13. Ge, S. J., Yao, X. L., Yang, Z. X., and Zhu, Z. P. (1998) *Cell Res.* **8,** 119–134
14. Zhang, J. Z., and Somerville, C. R. (1997) *Proc. Natl. Acad. Sci. U. S. A.* **94,** 7349–7355
15. Uwer, U., Willmitzer, L., and Altmann, T. (1998) *Plant Cell* **10,** 1277–1294
16. Ratcliff, F., Martin-Hernandez, A. M., and Baulcombe, D. C. (2001) *Plant J.* **25,** 237–245
17. Ahn, J. W., Kim, M., Kim, G. T., Lim, J. H., and Pai, H.-S. (2004) *Plant J.* **38,** 969–981
18. Cho, H. S., Lee, S. S., Kim, K. D., Kim, S. J., Hwang, I., Lim, J. S., Park, Y. I., and Pai, H.-S. (2004) *Plant Cell* **16,** 2665–2682
19. Lee, Y. J., Kim, D. H., Kim, Y.-W., and Hwang, I. (2001) *Plant Cell* **13,** 2175–2190
20. Porra, R. J., Thompson, W. A., and Kriedemann, P. E. (1989) *Biochim. Biophys. Acta* **975,** 384–394
21. Lilly, J. W., Havey, M. J., Jackson, S. A., and Jiang, J. (2001) *Plant Cell* **13,** 245–254
22. Burch-Smith, T. M., Anderson, J. C., Martin, G. B., and Dinesh-Kumar, S. P. (2004) *Plant J.* **39,** 734–746
23. Peeters, N., and Small, I. (2001) *Biochim. Biophys. Acta* **1541,** 54–65
24. Zhang, H., Huang, H. M., Carson, R. C., Mahmood, J., Thomas, H. M., and Gibson, G. E. (2001) *Anal. Biochem.* **298,** 170–180
25. Oubrahim, H., Stadtman, E. R., and Chock, P. B. (2001) *Proc. Natl. Acad. Sci. U. S. A.* **98,** 9505–9510
26. Kuroiwa, T., Suzuki, T., Ogawa, T., and Kawano, S. (1981) *Plant Cell Physiol.* **22,** 381–396
27. Sato, N. (2001) *Trends Plant Sci.* **6,** 151–155
28. Rowan, B. A., Oldenburg, D. J., and Bendich, A. J. (2004) *Curr. Genet.* **46,** 176–181
29. Oldenburg, D. J., and Bendich, A. J. (2004) *J. Mol. Biol.* **344,** 1311–1330
30. Chen, X., and Schnell, D. J. (1999) *Trends Cell Biol.* **9,** 222–227
31. Taylor, W. C. (1989) *Annu. Rev. Plant Physiol. Plant Mol. Biol.* **40,** 211–233
32. Austin, M. J., Muskett, P., Kahn, K., Feys, B. J., Jones, J. D. G., and Parker, J. (2002) *Science* **295,** 2077–2080
33. Azevedo, C., Sadanandom, A., Kitagawa, K., Freialdenhoven, A., Shirasu, K, and Schultze-Lefert, P (2002) *Science* **295,** 2073–2076
34. Liu, Y., Schiff, M., Serino, G., Deng, X.-W., and Dinesh-Kumar, S. P. (2002) *Plant Cell* **14,** 1483–1493
35. Garesse, R., and Vallejo, C. G. (2001) *Gene* (*Amst.*) **263,** 1–16
36. Butow, R. A., and Avadhani, N. G. (2004) *Mol. Cell* **14,** 1–15
37. Maréchal-Drouard, L., Weil, J. H., and Dietrich, A. (1993) *Annu. Rev. Plant Physiol. Plant Mol. Biol.* **44,** 13–32
38. Kumar, R. L., Maréchal-Drouard, L., Akama, K., and Small, I. (1996) *Mol. Gen. Genet.* **252,** 404–411
39. Glover K. E., Spencer, D. F., and Gray, M. W. (2001) *J. Biol. Chem.* **276,** 639–648
40. Duchene, A. M., and Marechal-Drouard, L. (2001) *Biochem. Biophys. Res. Commun.* **285,** 1213–1216
41. Miyata, S., Nakazono, M., and Hirai, A. (1998) *Curr. Genet.* **34,** 216–220
42. Sugiyama Y., Watase Y., Nagase M., Makita, N., Yagura, S., Hirai, A., and Sugiura, M. (2005) *Mol. Genet. Genomics* **272,** 603–615
43. Unseld, M., Marienfeld, J. R., Brandt, P., and Brennicke, A. (1997) *Nat. Genet.* **15,** 57–61
44. Kubo, T., Nishizawa, S., Sugawara, A., Itchoda, N., Estiati, A., and Mikami, T. (2000) *Nucleic Acids Res.* **28,** 2571–2576
45. Notsu, Y., Masood, S., Nishikawa, T., Kubo, N., Akiduki, G., Nakazono, M., Hirai, A., and Kadowaki, K. (2002) *Mol. Genet. Genomics* **268,** 434–445
46. Handa, H. (2003) *Nucleic Acids Res.* **31,** 5907–5916
47. Rokov-Plavec, J., Lesjak, S., Landeka, I., Mijakovic, I., and Weygand-Durasevic, I. (2002) *Arch. Biochem. Biophys.* **397,** 40–50
48. Osteryoung, K. W., and NcAndrew, R. S. (2001) *Annu. Rev. Plant Physiol. Plant Mol. Biol.* **52,** 315–333
49. Osteryoung, K. W., and Nunnari, J (2003) *Science* **302,** 1698–1704
50. Ibba, M., and Soll, D. (2002) *EMBO Rep.* **2,** 382–387
51. Lee, S. W., Cho, B. H., Park, S. G., and S. Kim (2004) *J. Cell Sci.* **117,** 3725–3734
52. Hanaoka, M., Kanamaru, K., Fujiwara, M., Takahashi, H., and Tanaka, K. (2005) *EMBO Rep.* **6,** 545–550
53. Oelmüller, R. (1989) *Photobiology* **49,** 229–239
54. Susek, R., Ausubel, F. M., and Chory, J. (1993) *Cell* **74,** 787–799
55. Lopez-Juez, E., Jarvis, P. R., Takeuchi, A., Page, A. M., and Chory, J. (1998) *Plant Physiol.* **118,** 803–815
56. Pfannschmidt, T. (2003) *Trends Plant Sci.* **8,** 33–41
57. Larkin, R. M., Alonso, J. M., Ecker, J. R., and Chory, J. (2003) *Science* **299,** 902–906
58. Strand, A., Asami, T., Alonso, J., Ecker, J. R., and Chory, J. (2003) *Nature* **421,** 79–82
59. Ahlert, D., Ruf, S., and Bock, R. (2003) *Proc. Natl. Acad. Sci. U. S. A.* **100,** 15730–15735
60. Ma, Z., and Dooner, H. K. (2004) *Plant J.* **37,** 92–103
61. Magnard, J. L., Heckel, T., Massonneau, A., Wisniewski, J. P., Cordelier, S., Lassagne, H., Perez, P., Dumas, C., and Rogowsky, P. M. (2004) *Plant Physiol.* **134,** 649–663